Cement and Concrete Research 42 (2012) 134–138

Contents lists available at SciVerse ScienceDirect

Cement and Concrete Research

journal homepage: http://ees.elsevier.com/CEMCON/default.asp

The early hydration of Ordinary Portland Cement (OPC): An approach comparing measured heat flow with calculated heat flow from QXRD

D. Jansen [a,*], F. Goetz-Neunhoeffer [a], B. Lothenbach [b], J. Neubauer [a,**]

[a] University Erlangen-Nuernberg, Mineralogy, Schlossgarten 5a, 91054 Erlangen, Germany
[b] Empa, Laboratory for Concrete and Construction Chemistry, Überlandstrasse 129, 8600 Dübendorf, Switzerland

ARTICLE INFO

Article history:
Received 19 April 2011
Accepted 13 September 2011

Keywords:
X-ray diffraction B
Calorimetry A
Hydration A
Kinetics A
Thermodynamic calculations B

ABSTRACT

Heat flow was calculated from XRD data and compared with measured heat flow from calorimetric experiments. It was shown that the heat released during the hydration of a commercial Ordinary Portland Cement can be assigned mainly to three mechanisms, the silicate reaction (sum of dissolution of alite and precipitation of C-S-H-phase and portlandite), the dissolution of C_3A, and the precipitation of ettringite. The contributions made by anhydrite dissolution and gypsum dissolution to the heat released during hydration turned out to be quite small. It is possible to explain, on the basis of the data produced, the origin of the heat flow curve of the cement used.

1. Introduction

Although Ordinary Portland Cements (OPC) have been the object of study for decades, the hydration process of OPCs still remains a subject of scientific debate. The hydration in question is quite a complex process which includes dissolution and precipitation reactions. One important unresolved question is how to explain the influence of different factors on the hydration kinetics, as visible in typical heat flow diagrams [1].

The process of the hydration of OPCs is commonly subdivided into several periods. These periods are called: the initial period (I), the induction period (II) the acceleration period (III) and the retardation period (IV) (Fig. 1). It is possible to sum up the acceleration period and the retardation period together under the denomination “main period”.

Many OPCs display two significant heat flow maxima during the main period. The first is attained several hours after the beginning of the acceleration period, while the second one appears during the deceleration period. The second heat flow maximum has already been described by Lerch [2] who calls it the “sulfate depletion peak”, due to the fact that its occurrence is a function of the sulfate content of the cement [3]. Hesse et al. [4] have confirmed the findings of Lerch and have been able to show that a renewed C_3A dissolution and an accelerated ettringite precipitation are the reasons for that additional heat flow which can be detected at the second heat flow maximum during the retardation period.

During early cement hydration, i.e. up to 20 h, two reactions, namely the silicate reaction (Eq. 1) and the aluminate reaction (Eq. 2), dominate the measured heat flow [5].

$$C_3S + 3.9\ H \rightarrow C_{1.7}SH_{2.6} + 1.3\ CH \text{ (silicate reaction)} \quad (1)$$

$$C_3A + 3\ Cs + 32\ H \rightarrow C_3A^{*}3Cs^{*}H_{32} \text{ ettringite (aluminate reaction)} \quad (2)$$

Recently it has been shown that a whole set of different approaches are all suitable for understanding the occurrence of the typical heat flow diagrams of hydrating cements or alite-water mixtures. Bishnoi and Scrivener have presented a new platform called μic [6] for the modeling of the hydration of cements, especially the microstructural evolution, and have implemented the platform successfully in order to clarify the development of heat during the hydration of alite [7]. They showed that, very often, nucleation and growth mechanisms can be used in order to reproduce reaction kinetics during the first 24 h of alite hydration. Thomas [8] has also modeled the nucleation and growth kinetics of alite using a mathematical “boundary nucleation” model and has successfully reproduced heat flow curves measured using an isothermal calorimeter. Hesse et al. [4] have made use of XRD data of cement pastes in order to calculate heat flow diagrams and have clarified the occurrence of a heat flow curve of a synthetic Portland Cement consisting only of alite, cubic C_3A and calcium sulfates. It is the intention of the present work to continue the research of Hesse et al. [4] and to apply it to the examination of the hydration of a commercial Portland Cement containing 12 phases. In comparison to Hesse et al. [4] dissolution and precipitation reactions of the aluminate reaction are treated separately in the present work.

* Corresponding author.
** Corresponding author. Tel.: +49 9131 85 23986; fax: +49 9131 85 23734.
E-mail addresses: DanHerJansen@googlemail.com (D. Jansen), neubauer.gzn@me.com (J. Neubauer).

0008-8846/$ – see front matter © 2011 Elsevier Ltd. All rights reserved.
doi:10.1016/j.cemconres.2011.09.001

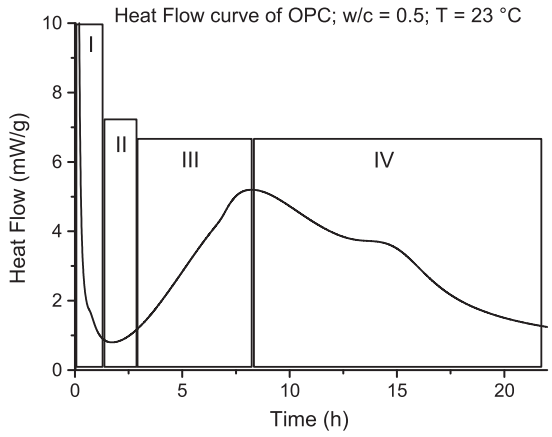

Fig. 1. Heat flow diagram of an Ordinary Portland Cement.

2. Materials and methods

2.1. Materials

Chosen for the experiments was a commercial Ordinary Portland Cement 52.5 R, which is used very often in the dry mix mortar industry. In order to ensure a proper detection of all phases in the OPC, minor phase enrichment experiments were performed [9, 10]. Representative samples for the experiments were obtained by means of the cone and quarter method. The chemical composition of the cement was measured using X-ray fluorescence and is shown in Table 1. The mineralogical composition of the cement is also shown in Table 1. The composition was determined via Rietveld refinement [11] using the fundamental parameters approach [12], the software Topas V4.2, and the G-factor method [13, 14]. The structures used for the Rietveld refinement and the respective ICSD codes are shown in Table 2. A detailed discussion concerning the amorphous content of a commercial OPC, as well as more literature about said topic, was reported elsewhere [14].

2.2. Experimental methods

Heat flow curves were measured using a commercial TAM Air calorimeter. Cement and water were weighed and equilibrated at 23 °C in an air-conditioned room. The mixing and stirring of the cement paste was carried out using an electric stirrer which allows a reproducible stirring (60 seconds). The preparation of the samples was performed outside the calorimeter at 23 °C in an air-conditioned room. The first minutes of the heat flow were not taken into account because of the slight disturbance of the signal caused by the opening of the calorimeter.

Table 1
Chemical and mineralogical composition of the cement used [31].

Phase	wt.%	Oxide	wt.%
Alite (C_3S)	57.7 ± 1.2	CaO	66.2
Belite (C_2S)	11.7 ± 0.6	SiO_2	22.6
α`-C_2S	8.0 ± 0.5	Al_2O_3	4.1
C_3A cubic	5.6 ± 0.3	Fe_2O_3	1.3
C_3A orthorhombic	4.8 ± 0.3	MgO	0.8
C_4AF	1.9 ± 0.2	K_2O	0.7
Gypsum	0.8 ± 0.1	Na_2O	0.1
Bassanite	1.5 ± 0.1	SO_3	3.4
Anhydrite	3.0 ± 0.2	LOI	0.8
Calcite	2.2 ± 0.2		
Quartz	0.9 ± 0.1		
Arcanite	0.9 ± 0.1		
Amorphous/misfitted	1.0 ± 0.5		

Table 2
Structures used for the Rietveld refinement [31].

Phase	ICSD Code	Reference
Alite (C_3S)	94742	De La Torre et al. [16]
Belite (C_2S)	963	Jost et al. [17]
α`-C_2S	-	Mueller [18]
C_3A_{cubic}	1841	Mondal and Jeffery [19]
$C_3A_{orthorhombic}$	100220	Takéuchi and Nishi [20]
C_4AF	51265	Jupe et al. [21]
Gypsum	27221	Pedersen et al. [22]
Bassanite	380286	Weiss and Bräu [23]
Anhydrite	16382	Kirfel and Will [24]
Calcite	80869	Maslen [25]
Quartz	174	Le Page and Donnay [26]
Arcanite	79777	Ojima et al. [27]
Ettringite	155395	Goetz-Neunhoeffer and Neubauer [28]
Portlandite	34241	Busing and Levy [29]
Silicon	51688	Többens et al. [30]

Cement pastes were also examined in-situ by means of X-rays using a D8 diffractometer from Bruker AXS equipped with a Lynx Eye position-sensitive detector. We made use of CuKα radiation at 40 kV and 40 mA and recorded from 7° 2θ to 40° 2θ, with a step width of 0.0236° 2θ and 0.58 s, counting time per step. Under these data acquisition conditions, it is possible to record 88 ranges within the first 22 h of hydration. The Rietveld [11] software used was Topas 4.2 from Bruker AXS. The intensity caused by the Kapton polyimide film was fitted with a specific model. To this end the Kapton film was stretched over a single crystal sample holder and the pattern of the Kapton film was fitted with a peaks phase which was later implemented into the refinement of the cement paste [15]. All structure models used for the Rietveld refinement are shown in Table 2. The composition of the cement paste was determined over time via Rietveld refinement of the XRD patterns of the cement paste using the calculated scale factors from Rietveld refinement for the G-factor method [31].

The G-factor method is based on the calculation of a calibration constant for the diffractometer using a standard material (in our case silicon [31]).

$$G = s_{si}\frac{\rho_{si}V_{si}^2\mu_{si}^*}{c_{si}}$$

where

S_{Si}	Rietveld scale factor of silicon from Rietveld analysis
ρ_{Si}	Density of silicon
V_{Si}	Unit-cell volume of silicon
C_{Si}	Weight fraction of silicon (100 wt.%)
μ^*_{Si}	Mass attenuation coefficient of silicon

The factor G is then used in order to calculate the amount of each single crystalline phase in the cement paste, taking into account the density of each phase j (ρ_j), the unit-cell volume of each phase j (V_j), the calculated scale factor for each phase j (s_j) and the mass attenuation coefficient of the whole sample μ^*_{SAMPLE} (68.7 cm^2/g) which in our case was determined from XRF data (dry cement 97.9 cm^2/g; water 10.3 cm^2/g; w/c = 0.5).

$$c_j = s_j\frac{\rho_j V_j^2\mu^*_{SAMPLE}}{G}$$

A detailed discussion and evaluation of the method is given elsewhere [14, 31].

2.3. Calculation of the reaction enthalpies

It has been demonstrated by Hesse et al. [4] that the heat generated by the reaction of alite and aluminate with calcium sulfates can be

calculated from the experimentally determined dissolution, and from the enthalpies, of the different solids. The calculated heat flow curves help us to understand the respective contributions of the different reactions to the typical heat flow curves of alite and aluminate. In the present paper more precise calculations were carried out in order to understand the contribution of the different dissolution and precipitation reactions to the heat flow measured during the hydration of an OPC.

As a first step, the most likely reactions in the cement paste during hydration had to be identified: The two main reactions during the hydration of cements are the silicate reaction and the aluminate reaction (Eq. (1) and Eq. (2)). While the dissolution of alite (Eq. (1)) seems to result directly in the simultaneous formation of equimolar amounts of C-S-H and portlandite (see chapter results and [32]), the dissolution reactions of C_3A and calcium sulfates (Eq. 2) do not occur isochronously with the precipitation of ettringite (see chapter results and ref. [31]). Therefore, the heat contribution of the silicate reaction can be calculated representatively using the determined amount of C_3S reacted in the cement paste (thermodynamic calculations indicate that the contribution of the dissolved species in a 1:1 H_2O:C_3S mixture is less than 1% compared to the total heat of the reaction). Based on the experimental observations, however, the aluminate and calcium sulfate reaction has to be subdivided into several dissolution and precipitation reactions.

As the reactions take place in an OPC paste, where pH values in the range of 13 to 13.5 are present, the dissolution and precipitation reactions given below all refer to a pH value of 13.3. At this pH, the predominant aqueous species are $Al(OH)_4^-$, SO_4^{2-}, OH^-, Ca^{2+} and $CaOH^+$ (roughly 50% Ca^{2+} and 50% $CaOH^+$). Thus, the following equations are used to calculate the dissolution of aluminate, anhydrite and gypsum and the precipitation of ettringite in an OPC:

$$C_3A + 6\ H_2O \rightarrow 2\ Al(OH)_4^- + 2.5\ OH^- + 1.5\ Ca^{2+} + 1.5\ CaOH^+ (\text{Dissolution } C_3A) \quad (3)$$

$$3CaSO_4 + 1.5\ OH^- \rightarrow 1.5Ca^{2+} + 1.5\ Ca(OH)^+ + 3SO_4^{2-} (\text{Dissolution anhydrite}) \quad (4)$$

$$3CaSO_4^*2H_20 + 1.5\ OH^- \rightarrow 1.5Ca^{2+} + 1.5\ Ca(OH)^+ + 3SO_4^{2-} + 6\ H_2O (\text{Dissolution gypsum}) \quad (5)$$

$$3\ Ca^{2+} + 3\ CaOH^+ + 2\ Al(OH)_4{}^- + 3\ SO_4{}^{2-} + 2.5\ OH^- + 26\ H_2O \rightarrow \text{Ettringite} + 1.5\ OH^- (\text{Precipitation ettringite}) \quad (6)$$

The enthalpies of reaction for all equations are shown in Table 3. The enthalpies were calculated using the enthalpies of the different solids and the dissolved species as given in the GEMS version of Nagra/PSI thermodynamic database [33], the cemdata07 database [34] (for ettringite, alite and aluminate) and in Fuji and Kondo [35] for the enthalpy of formation for $C_{1.7}SH_{2.6}$. The thermodynamic software GEMS [36] was used to calculate the speciation at pH 13.3 and the enthalpies at 23 °C.

Table 3
Enthalpies of reaction for the assumed reactions.

Reaction	Enthalpy
Eq. (1) (Silicate reaction)	−561 J/g_{Alite}
Eq. (3) (Dissolution C_3A)	−868 J/g_{C3A}
Eq. (4) (Dissolution anhydrite)	−50 J/$g_{Anhydrite}$
Eq. (5) (Dissolution gypsum)	59 J/g_{Gypsum}
Eq. (6) (Precipitation ettringite)	−214 J/$g_{Ettringite}$

The calculation of heat flow curves from XRD data was carried out according to the following pattern (modified in accordance with Hesse et al., 2011 [4]) and the values given in Table 3.

$$HF = \frac{\frac{\partial\ \text{wt.}-\%\ \text{phase}}{\partial t}}{100} \times \Delta HR \times (-1) \quad (7)$$

where

$\frac{\partial\ \text{wt.}-\%\text{alite}}{\partial t}$ Derivative of the phase content curves

ΔH_R Enthalpy of reaction

3. Results

Fig. 2 shows the heat flow of the cement paste as obtained from the heat flow experiments, as well as the phase content of alite as determined by means of X-ray diffraction.

It can be seen that the dissolution of alite commences at the beginning of the acceleration period. The thin line in Fig. 2 shows the heat flow calculated from the alite dissolution curve determined by in situ X-ray diffraction. It was already shown that the dissolution of alite is suitable for characterizing the kinetics of the reaction of pure alite with water [32]. Hence, it can be assumed that the heat flow contribution of the silicate reaction corresponds to the thin line.

We assume that the precipitation of the C-S-H phase appears synchronously with the alite dissolution, as observed in the case of portlandite, even though the C-S-H phase was not quantified by means of X-rays due to the low degree of crystallinity. Indeed, C-S-H precipitation can occur before portlandite precipitation within the nucleation process, but with negligible quantity.

The measured heat flow curve of the cement used, combined with the phase contents of the phases ettringite as well as C_3A and the heat flows calculated from the phase content curves of ettringite and C_3A are shown in Fig. 3. The heat flow contributions of anhydrite dissolution and gypsum dissolution are negligible as shown in Fig. 4.

If one compares the amount of C_3A in the dry cement and the w/c-ratio of the paste examined it is conspicuous here that around 1.8 wt.% of C_3A are dissolved immediately during mixing the cement with water while only 2.7 wt.% of ettringite are precipitated. Taking into account Eq. (2) almost 8 wt.% of pure ettringite can be precipitated with the amount of 1.8 wt.% of dissolved C_3A.

Results clearly showed that, in the case of the aluminate reaction, it would be incorrect to assume that the heat contribution of the C_3A

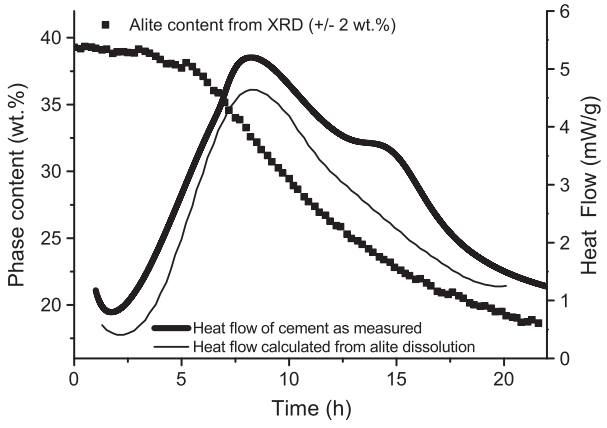

Fig. 2. Alite content during cement hydration determined by means of X-ray diffraction, heat flow calculated from X-ray results and heat flow of the cement used measured with a heat flow calorimeter (XRD results from ref. [31]).

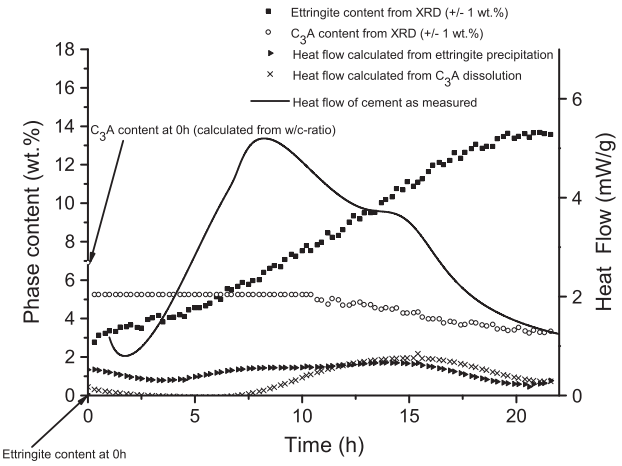

Fig. 3. Ettringite and C_3A contents during cement hydration determined by means of X-ray diffraction, heat flow calculated from X-ray results and heat flow of the cement used measured with a heat flow calorimeter (XRD results from ref. [31]).

dissolution is representative also for the amount of precipitated ettringite determined in the cement paste [31].

Besides that, precipitation of ettringite does not signify the dissolution of C_3A and sulfate carrier at the same point of time as formulated in Eq. 2 [31]. C_3A dissolution ceases after the initial dissolution and recommences after 12 h, whereas ettringite is formed continuously from the point of beginning measurement up to 22 h of hydration [31].

It can be seen from Fig. 3 that the heat flow maximum at 15 h is mainly characterized by the heat caused by the dissolution of C_3A. The heat from ettringite precipitation contributes to the heat flow over the whole main period.

All calculated heat flow curves shown were computed using the enthalpy data given in Table 3.

Fig. 4 shows the heat flow curve of the cement as measured by means of isothermal heat flow calorimetry (TAM Air) along with the heat flow curves as calculated from the XRD data. It can be seen that the calculated heat flow matches the measured heat flow reasonably well. The heat released during the first maximum of heat flow (here called the "silicate reaction peak") is mainly to be attributed to the heat released from the silicate reaction, which in our case includes the dissolution of the phase alite and the precipitation of portlandite and C-S-H phase.

The second heat flow maximum, occurring after about 15 h (here called the "sulfate depletion peak") is characterized by the fact of the heat's being released due to the dissolution of C_3A and the precipitation of ettringite, even though the silicate reaction still contributes significantly (about 2 mW/g) to the heat flow, which reaches, at the point of the second maximum, a level of 3.8 mW/g.

The contributions of the anhydrite dissolution and the gypsum dissolution to the heat flow are negligible in comparison with the contributions made by the other reactions.

4. Discussion

On the basis of the data here presented, we may conclude that the two maxima occurring during the main period of cement hydration can be assigned to different reactions. It should be noted that the following statements are validated only for the cement used in the present study. Other cements might react in other ways and therefore might display maxima pronounced to different degrees.

Fig. 5 shows the heat flow curve, as measured, of the cement used, together with the calculated total heat of hydration, also taking into account the partial contributions to the heat flow of the silicate reaction, C_3A dissolution and ettringite precipitation. Neither the contribution made by gypsum dissolution nor that made by anhydrite dissolution were taken into account, since both of these contributions were so small as to be negligible.

Excluding the initial period of cement hydration (up to the 60 minute-point) approximately 230 J/g ± 8 J/g of heat of hydration could be measured during the main period of cement hydration. We can sub-divide this amount of measured heat into approximately 127 J/g during the silicate reaction peak and 103 J/g during the sulfate depletion peak.

Whereas the silicate reaction and the ettringite formation contribute to both—i.e. to the silicate reaction peak as well as to the sulfate depletion peak—the dissolution of the C_3A contributes to the sulfate

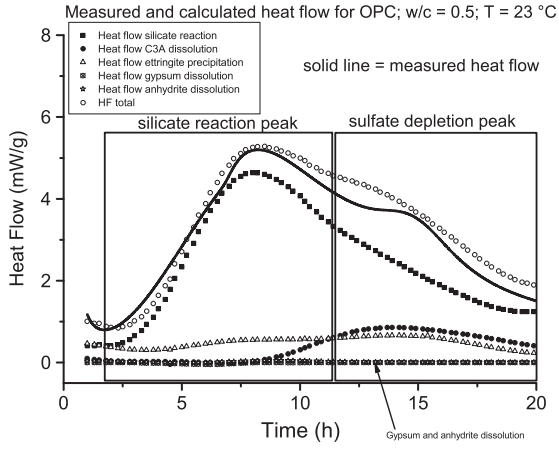

Fig. 4. Comparison between calculated heat flow and measured heat flow.

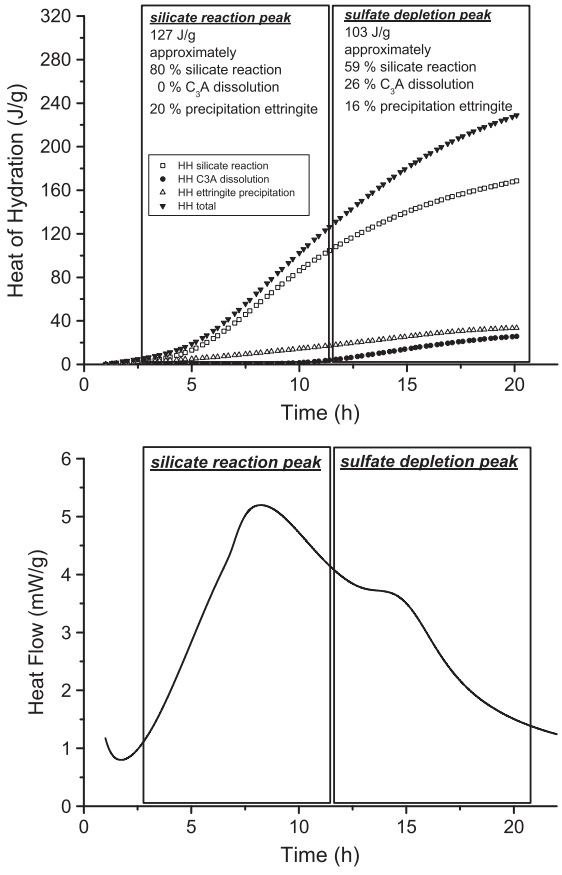

Fig. 5. Heat flow and total heat of hydration during the hydration of the OPC used.

depletion peak alone. More than 41% of the heat released during the sulfate depletion peak can be attributed to the aluminate reaction.

Since there is no further reaction of the C_3A detectable until the sulfate depletion peak occurs, it is conceivable that the amount of C_3A which reacts immediately after mixing the cement with water is sufficient to produce the precipitation of ettringite until further dissolution of C_3A can be detected. The dissolution of 1.7 wt.% of C_3A during stirring of the paste and the first XRD pattern after 15 minutes was observed. But only 2.8 wt.% of ettringite are precipitated at the same interval. The 2.0 wt.% of dissolved C3A are sufficient for the precipitation of approximately 9 wt.% of pure ettringite (considering Eq. 2). These 9 wt.% correspond approximately to the amount of ettringite precipitated at the point in time at which the further dissolution of C_3A begins. We might assume that an amorphous aluminate phase is formed during the first minutes of cement hydration which then serves as a reservoir for the consequent ettringite formation. It might be interesting to perform some AI^{27} NMR experiments in order to verify whether such an Al-reservoir actually exists.

The data yielded by this investigation show that the first maximum occurring during the main period, namely at about 7.5 h, is accompanied by a change in the controlling mechanism of the silicate reaction. The transition from the acceleration period to the deceleration period in the heat flow of the hydrating cement is in very good accordance with the transition from the acceleration period to the deceleration period in the silicate reaction, even though the ettringite precipitation also contributes to the heat measured at this maximum.

Since the further reaction of the C_3A and the accelerated ettringite precipitation strongly depends on the presence (amount and reactivity) of the sulfate carriers [2, 3, 4, 31], the heat flow maximum occurring during the deceleration period (we say this even though the maximum in question does not always occur during the deceleration period) is designated as the "sulfate depletion" peak [2]. The heat flow as measured is caused by the silicate reaction, C_3A dissolution and accelerated ettringite precipitation. However, the accelerated ettringite precipitation in our system is not as pronounced as it is in other systems [4].

Acknowledgements

The authors would like to thank Florian Deschner for his support.

References

[1] J. W. Bullard, H. M. Jennings, R. A. Livingston, A. Nonat, G. W. Scherer, J. S. Schweitzer, K. L. Scrivener, J. J. Thomas, Mechanisms of cement hydration, Cement and Concrete Research, In Press, Corrected Proof, Available online 29 October 2010, ISSN 0008–8846, DOI: 10.1016/j.cemconres.2010.09.011.
[2] W. Lerch, The influence of gypsum on the hydration and properties of Portland cementpastes, Am. Soc. Test. Mater. 46 (1946) 1252–1297.
[3] P. Sandberg, L.R. Roberts, Studies of cement–admixture interactions related to aluminate hydration control by isothermal calorimetry, Am. Concr. Inst. 217 (2003) 529–542.
[4] C. Hesse, F. Goetz-Neunhoeffer, J. Neubauer, A new approach in quantitative in-situ XRD of cement pastes: Correlation of heat flow curves with early hydration reactions, Cem. Concr. Res. 41 (2010) 123–128.
[5] H.F.W. Taylor, Cement Chemistry, 2nd ed Thomas Telford Publishing, 1997.
[6] S. Bishnoi, K.L. Scrivener, μic: a new platform for modeling the hydration of cements, Cem. Concr. Res. 39 (2009) 266–274.
[7] S. Bishnoi, K.L. Scrivener, Studying nucleation and growth kinetics of alite hydration using μic, Cem. Concr. Res. 39 (2009) 849–860.
[8] J.J. Thomas, A new approach to modeling the nucleation and growth kinetics of tricalcium silicate hydration, J. Am. Ceram. Soc. 90 (2007) 3282–3288.
[9] W.A. Gutteridge, On the dissolution of the interstitial phases in Portland cement, Cem. Concr. Res. 9 (1979) 319–324.
[10] L.J. Struble, The effect of water on maleic acid and salicylic acid extractions, Cem. Concr. Res. 15 (1985) 631–636.
[11] H.M. Rietveld, A profile refinement method for nuclear and magnetic structures, J. Appl. Crystallogr. 2 (1969) 65–71.
[12] R.W. Cheary, A. Coelho, A fundamental parameters approach to X-ray line-profile fitting, J. Appl. Crystallogr. 25 (1992) 109–121.
[13] B.H. O´Connor, M.D. Raven, Application of the Rietveld Refinement Procedure in Assaying Powdered Mixtures, Powder Diffr. 3 (1988) 2–6.
[14] D. Jansen, Ch. Stabler, F. Goetz-Neunhoeffer, S. Dittrich, J. Neubauer, Does Ordinary Portland Cement contain amorphous phase? A quantitative study using an external standard method, Powder Diffr. 26 (2011) 31–38.
[15] C. Hesse, F. Goetz-Neunhoeffer, J. Neubauer, M. Braeu, P. Gaeberlein, Quantitative in situ X-ray diffraction analysis of early hydration of Portland cement at defined temperatures, Powder Diffr. 24 (2009) 112–115.
[16] A.G. De La Torre, S. Bruque, J. Campo, M.A.G. Aranda, The superstructure of C_3S from synchrotron and neutron powder diffraction and its role in quantitative phase analysis, Cem. Concr. Res. 32 (2002) 1347–1356.
[17] K.H. Jost, B. Ziemer, R. Seydel, Redetermination of the structure of β-dicalcium silicate, Acta Crystallogr., Sect. B: Struct. Crystallogr. Cryst. Chem. 33 (1977) 1696–1700.
[18] R. Mueller, Stabilisierung verschiedener Dicalciumsilikat-Modifikationen durch den Einbau von Phosphat: Synthese, Rietveld-analyse, Kalorimetrie, Diplomathesis (2001) University of Erlangen.
[19] P. Mondal, J. Jeffery, The crystal structure of tricalcium aluminate, $Ca_3Al_2O_6$, Acta Crystallogr., Sect. B: Struct. Crystallogr. Cryst. Chem. 31 (1975) 689–697.
[20] Y. Takéuchi, F. Nishi, Crystal-chemical characterization of the Al_2O_3–Na_2O solid-solution series, Z. Kristallogr. 152 (1980) 259–307.
[21] A.C. Jupe, J.K. Cockcroft, P. Barnes, S.L. Colston, G. Sankar, C. Hall, The site occupancy of Mg in the brownmillerite structure and its effect on hydration properties: an X-ray/neutron diffraction and EXAFS study, J. Appl. Crystallogr. 34 (2001) 55–61.
[22] B.F. Pedersen, Neutron diffraction refinement of the structure of gypsum, Acta Crystallogr., Sect. B, Struct. Crystallogr. Cryst. Chem. 38 (1982) 1074–1077.
[23] H. Weiss, M.F. Bräu, How much water does calcined gypsum contain? Angew. Chem. Int. Ed. 48 (2009) 3520–3524.
[24] A. Kirfel, G. Will, Charge density in anhydrite $CaSO_4$, from X-ray and neutron diffraction measurements, Acta Crystallogr., Sect.B: Struct. Crystallogr. Cryst. Chem. 36 (1980) 288–2890.
[25] E.N. Maslen, V.A. Streltsov, N.R. Streltsova, Electron density and optical anisotropy in rhombohedral carbonates. III. Synchroton X-ray studies of CaCO3, MgCO3 and MnCO3, Acta Crystallogr., Sect. B: Struct. Sci. 51 (1995) 929–939.
[26] Y. Le Page, G. Donnay, Refinement of the crystal structure of low-quartz, Acta Crystallogr., Sect.B: Struct. Crystallogr. Cryst. Chem. 32 (1976) 2456–2459.
[27] K. Ojima, Y. Hishihata, A. Sawada, Structure of potassium sulfate at temperatures from 296 K down to 15 K, Acta Crystallogr., Sect. B: Struct. Sci. 51 (1995) 287–293.
[28] F. Goetz-Neunhoeffer, J. Neubauer, Refined ettringite structure for quantitative X-ray diffraction analysis, Powder Diffr. 21 (2006) 4–11.
[29] W.R. Busing, H.A. Levy, Neutron diffraction study of calcium hydroxide, Acta Crystallogr., Sect. B: Struct. Sci. 42 (1986) 51–55.
[30] D.M. Többens, N. Stuesser, K. Knorr, H.M. Mayer, G. Lampert, The new high-resolution neutron powder diffractometer at the Berlin neutron scattering center, Mater. Sci. Forum 378 (2001) 288–293.
[31] D. Jansen, F. Goetz-Neunhoeffer, Ch. Stabler, J. Neubauer, A remastered external standard method applied to the quantification of early OPC hydration, Cem. Concr. Res. 41 (2011) 602–608.
[32] D. Jansen, S.T. Bergold, F. Goetz-Neunhoeffer, J. Neubauer, The hydration of alite: a time-resolved quantitative X-ray diffraction approach using the G-factor method compared with heat release, J. Appl. Cryst. 44 (2011) 895–901.
[33] D. Kulik, GEMS-PSI 3.0available at, http://gems.web.psi.ch/2010PSI-Villigen, Switzerland.
[34] B. Lothenbach, T. Matschei, G. Möschner, F.P. Glasser, Thermodynamic modeling of the effect of temperature on the hydration and porosity of Portland cement, Cem. Concr. Res. 38 (1) (2008) 1–18.
[35] K. Fuji, W. Kondo, Communications of the American ceramic society: Estimation of thermochemical data for calcium silicate hydrate (C-S-H), J. Am. Ceram. Soc. 66 (1983) C-220–C-221.
[36] W. Hummel, U. Berner, E. Curti, F.J. Pearson, T. Thoenen, Nagra/PSI Chemical Thermodynamic Data Base 01/01, USA, also published as Nagra Technical Report NTB 02–16, Universal Publishers/uPUBLISH.com, Wettingen, Switzerland, 2002 565.